CHAPTER 3
THE IMAGE PROCESSING SYSTEM

This chapter outlines the image processing system employed in this study. The selection of both hardware and software components of the system is presented, and the numerical procedures developed for measuring two–dimensional material deformations are described. The software is presented with regard to the two-roll milling of prepared cane or bagasse and was created using images from a preliminary two–roll bagasse milling experiment. Elaborations are made in regard to software developments for other forms of experimentation and measurement improvements. All software was written and compiled in FORTRAN 77 syntax.

3.1 Overview of the image processing system

The digital image processing system created for this study consists primarily of hardware components for image capture and storage, and software tools for preparation and treatment of the image data. Figure 3.1 shows the breakdown of the system.

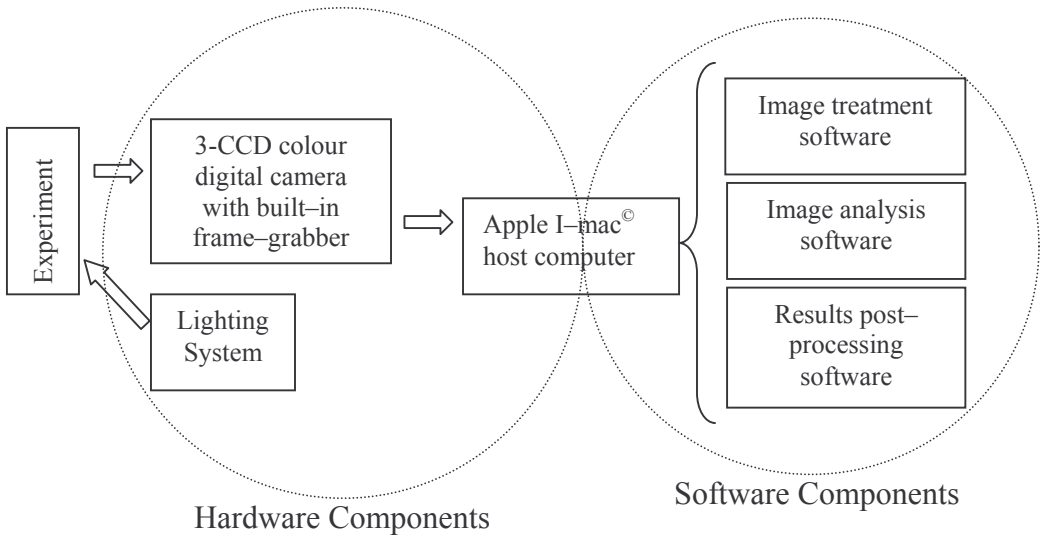

Figure 3.1. The digital image processing system.

3.2 Lighting system

A two–thousand Watt quartz tungsten halogen studio lamp was employed in an incident light illumination arrangement to illuminate an external surface of experimental samples. The light source was chosen due to its following properties:

1. Provides even spatial and temporal light intensity over the sample.
2. Sufficient light intensity to provide a quality image.
3. Suitably durable for the experimental application.
4. Readily available at low cost.

Incident light illumination was selected for the following reasons:

1. Cane and bagasse fibre is suitably light in colour for scattered light illumination.
2. At a suitable incident angle, there is no light reflection on the lens.
3. Simple to implement in the experimental environment.

3.3 CCD camera

Versatility and budget played important roles in selection of the CCD camera for this study. The aim was to select a good quality digital camera for practical use in many experimental environments. Whilst image measurement for analysis requires only monochrome images, a colour camera was desired for visualisation of experiments. In light of these requirements, a Sony DCR-TRV 900 3-CCD colour digital camera with built-in frame grabbing hardware was purchased. This unit produces digital images that are 768 pixels by 576 pixels in dimension, at a frame rate of 25 fps (frames per second). This camera provides various modes of operation, from completely manual to fully automatic settings. The camera zoom lens has a variable focal range of (L_f = 4.3 to 51.6 mm), which converts to a standard 35 mm film camera range of ($L_{f\ 35mm}$ = 41 to 492 mm). The corresponding range in photographic angle for the lens is (υ = 4.4° to 49.9°). The Sony DCR–TRV 900 has I–Link IEEE–1394 firewire© interface for connection to a host computer.

3.4 Host computer

The hardware function of the host computer is to accept and store the digital images from the CCD camera. An Apple I-mac© computer was selected for this application due to excellent graphical performance and built-in IEEE–1394 firewire© hardware for high–speed data transfer. The CCD camera is connected to the host computer via

a connection to the IEEE–1394 firewire© card, and the incoming image data is managed by I–movie2© streaming video software and stored in the computer RAM.

3.5 Image treatment

The I–movie2© software controls the camera via the IEEE–1394 connection and allows the user to start/stop the import of streaming digital video. Footage of an experiment is imported and stored on the computer as a video clip, consisting of twenty-five 768 pixel x 576 pixel frames per second. The I–movie2© software also provides a variety of editing tools, that allow the trimming of captured video clips on a frame-to-frame basis. Thus, in the case of experimental footage, the unwanted sections (generally the beginning and end) of the video file are discarded, prior to exporting the video file. The I–movie2© export tool allows the export of a streaming video file in the form of a 256-greyscale Quicktime© movie file (.mov) with user specified frame rate.

The exported 256–greyscale movie file is decomposed into a time series of digital TIFF (tagged image file format) images, the number of which corresponds to the length of the video clip and the frame rate specified. The resulting image series is passed to NIH© image software using a customised macro script, that rewrites the image header for compatibility with the image reading subroutine that is employed within the FORTRAN image analysis software. The image series is then ready for image measurement analysis.

3.6 Image Analysis

Image analysis software was designed specifically for analysis of both continuous (two-roll milling) and transient (uniaxial compression) process experiments. Examples of the images captured for these two experimental regimes are shown in Figure 3.2.

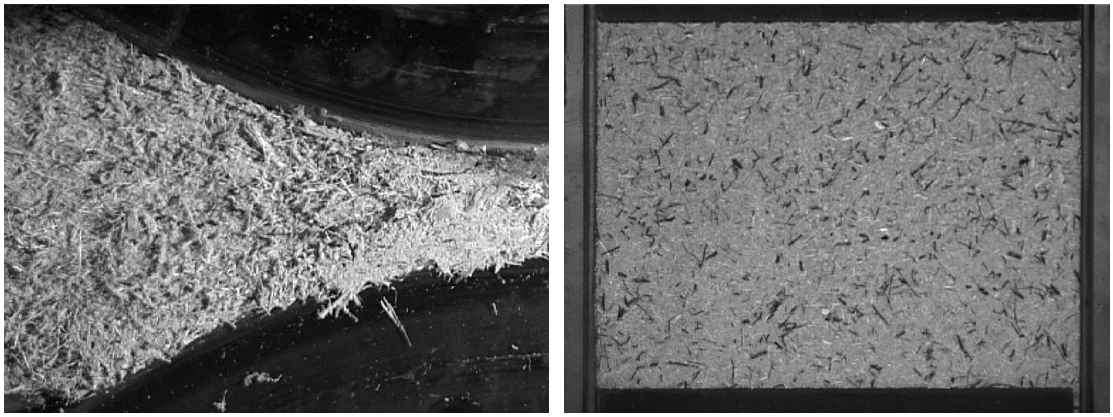

Figure 3.2. Images from two–roll milling and confined uniaxial compression experiments.

The major aim of the software is to directly measure kinematic quantities from a two–dimensional material surface. The documentation of the image analysis software will present the simplest case of two-roll milling as a base description of the software and elaborate on the evolution of the codes for application to the completely transient process of uniaxial compression. The theory of the analysis procedure (termed *Image Tensor Analysis* or ITA) is presented, along with the relative implementation of this theory within the software.

3.6.1 The ITA procedure

The procedure of ITA involves taking video footage of a process experiment, such as the two-roll milling of bagasse. Video footage of an experiment is decomposed into a time series of adjacent grey–scale TIFF images. The TIFF images are read by the FORTRAN subroutine read_tiff (Harris 1992) as a two–dimensional (X, Y) array of pixel intensity values. A particle-tracking algorithm was created to track points (or nodes) assigned to a material surface and store the location of each point spatially at all available times (that is, the location of each grid point in each image of the selected image series). This temporal location data forms the deformation function ($\widetilde{\chi}$) as explained in Section 2.7.

Finite differencing of the deformation function is then conducted in order to obtain the partial differentials of nodal locations with respect to the reference configuration. For means of simplicity, the initial grid location is chosen as the reference configuration for the section of material being analysed. Gathered as a tensor, these spatial derivatives form the deformation gradient ($\widetilde{F}$). This is perhaps the most

fundamental of kinematic quantities in continuum mechanics and forms the basis for calculation of the right Cauchy-Green deformation tensor ($\widetilde{C}$) (Truesdell 1966), which describes the stretch of the body. Further algebraic manipulation is required to determine the desired modes of material strain from the Doyle-Erickson family of Lagrangian finite-strain tensors. Figure 3.3 contains a flow chart of the ITA numerical procedure.

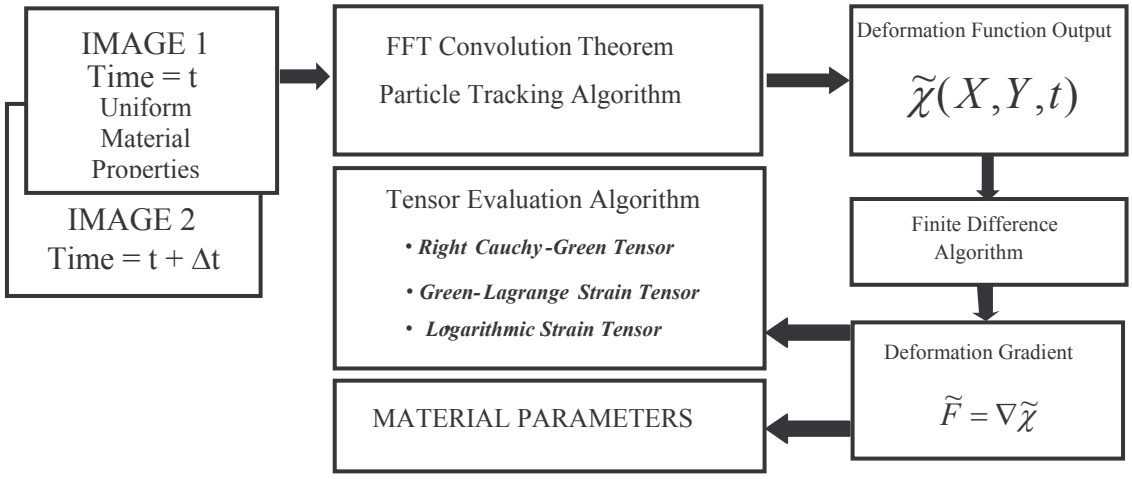

Figure 3.3. Flow chart illustrating the ITA numerical procedure.

3.6.1.1 The particle–tracking algorithm

The particle-tracking algorithm uses the first pair of adjacent images in an image series, as initial input. On the first of these images, the initial nodal locations of a three-column grid are identified. This initial configuration has been chosen as the reference configuration, i.e. The pixel configuration of the body points in the X,Y image plane at the time datum. Only a simple mathematical transformation is required in order to describe the deformations in terms of some other reference configuration. Placement of the analysis grid is illustrated in Figure 3.4.

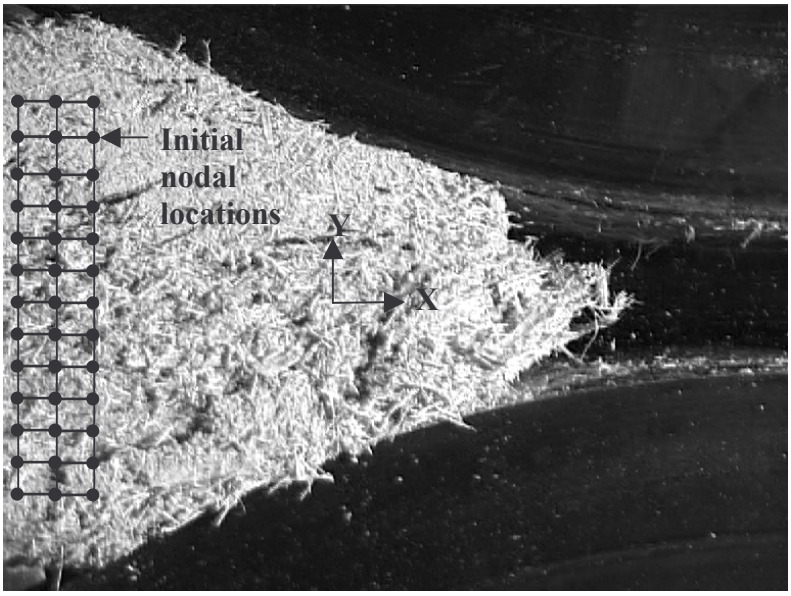

Figure 3.4. Placement of the three-column grid for analysis of two-roll milling experiments.

Sub-regions of analysis are placed centrally over the initial nodal locations. The subroutine fourn.f (Press et al. 1992) is employed to determine the cross–correlation plane for square sub–regions with a side length of 2^n pixels (i.e. 2, 4, 8, 16, 32, 64,.., 2^n). The location of the displacement peak in the correlation template is determined to single pixel accuracy, via the maximum correlation coefficient (Harris 1992). If the maximum correlation coefficient for a sub–region is less than 0.63, the program is flagged and aborted. A parabolic three–point estimator is then employed to measure the displacement to sub–pixel accuracy (Westerweel 1993, Stephens 1996). The resulting pixel displacements are added to the initial location of each node, and its new pixel location in the X,Y image plane stored in multi–dimensional arrays. It is this temporal location data that forms the deformation function Chi ($\tilde{\chi}$). The sub–region associated with each node is then relocated to its new location, and the procedure repeated. The motion is converted from pixels to a physical scale such as millimetres, via a scaling factor. Scaling is conducted post finite–differencing of the motion, in order to eliminate the growth of possible scaling errors.

For real-time tracking the program will in each iteration, disregard the first image from the previous pair and gather the next image in the series, hence following the same section of material through space and time. Alternatively, the assumption of

steady state conditions can be made, allowing the deformation function to be obtained directly from a single image pair.

3.6.1.2 The finite difference algorithm

The finite difference algorithm is employed in order to obtain the deformation gradient ($\widetilde{F}$) in two-dimensions:

$$\widetilde{F} = \nabla \widetilde{\chi}_{\widetilde{\kappa}} = \begin{bmatrix} \frac{\partial x}{\partial X} & \frac{\partial y}{\partial X} \\ \frac{\partial x}{\partial Y} & \frac{\partial y}{\partial Y} \end{bmatrix} \qquad \text{(EQ 3.1)}$$

The partial differentials of the nodal x, y positions, with respect to their X, Y counterparts in the reference configuration are approximated using central, forward and backward differencing techniques involving second order Taylor's Series expansions (Section 2.8). This procedure is illustrated for three points in a simple nine-point analysis grid in Figure 3.5.

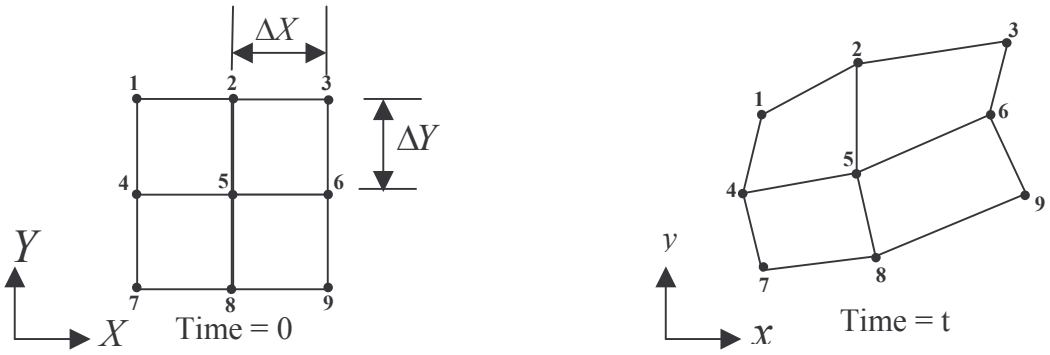

Examples of second order three-point approximations at time (t)

Three-point centred - Point (5): $\left(\frac{\partial x}{\partial X}\right)_5 = \frac{(x_6 - x_4)}{2\Delta X}$

Three-point forward - Point (8): $\left(\frac{\partial y}{\partial Y}\right)_8 = \frac{(-3y_8 + 4y_5 - y_2)}{2\Delta Y}$

Three-point backward - Point (6): $\left(\frac{\partial x}{\partial Y}\right)_6 = \frac{(-3x_6 + 4x_5 - x_4)}{2\Delta Y}$

Figure 3.5. Central, forward and backward three-point second order approximations for components of the deformation gradient.

The finite difference algorithm utilises individual software loops to calculate the forward and backward approximations for nodes on each of the four mesh boundaries and a separate loop to determine the central difference approximations for nodes in the centre column of the analysis grid. The components of the time rate of the deformation gradient ($\dot{\tilde{F}}$) are evaluated using second order Taylor series expansions to approximate the temporal derivatives of the four components of $\tilde{F}$, for each node in the grid, at all available points in time.

3.6.1.3 Tensor algebra

Once the deformation gradient has been obtained, the Right Cauchy-Green deformation tensor ($\tilde{C}$) is determined as shown.

$$\tilde{C} = \tilde{F}^T \tilde{F} \qquad \text{(EQ 3.2)}$$

The eigenvalues of the Right Cauchy-Green deformation tensor are the squares of the principal stretch ratios (λ_i), and its eigenvectors, are the directions of these principal stretches. The principal stretches form the right stretch tensor ($\tilde{U}$), which is governed by the polar decomposition of the deformation gradient ($\tilde{F}$), such that:

$$\tilde{F} = \tilde{R}\tilde{U} \qquad \text{(EQ 3.3)}$$

where ($\tilde{R}$) is a two-dimensional rotation tensor,

$$\tilde{R} = \begin{bmatrix} \cos\theta & -\sin\theta \\ \sin\theta & \cos\theta \end{bmatrix} \qquad \text{(EQ 3.4)}$$

with (θ) defining the angle of rotation between the reference and eigensystem coordinate axes. Hence, in two dimensions,

$$\tilde{C} = \tilde{U}^2 = \begin{bmatrix} \lambda_1^{\,2} & 0 \\ 0 & \lambda_2^{\,2} \end{bmatrix} \qquad \text{(EQ 3.5)}$$

The Doyle-Erickson family of Lagrangian finite strain tensors are defined by the following general equation

$$\widetilde{\varepsilon}^{m} = \begin{cases} \frac{1}{m}(\widetilde{U}^{m} - \widetilde{I}) & m \neq 0 \\ \ln(\widetilde{U}) & m = 0 \end{cases} \qquad \text{(EQ 3.6)}$$

where ($\widetilde{I}$) denotes the identity tensor. The members of the Doyle-Erickson family of finite strain tensors that are of importance to measurement of material strain in the ITA procedure are those conventionally output by finite element solutions and are listed with their respective indices below.

m=0; Hencky's or logarithmic strain: $\widetilde{\varepsilon}^{0} = \frac{1}{0}(\widetilde{U}^{0} - \widetilde{I}) = \ln(\lambda_i)$ (EQ 3.7)

m=1; Biot's or nominal strain: $\widetilde{\varepsilon}^{1} = (\widetilde{U} - \widetilde{I}) = \lambda_i - 1$ (EQ 3.8)

m=2; Green's strain: $\widetilde{\varepsilon}^{2} = \frac{1}{2}(\widetilde{U}^{2} - \widetilde{I}) = \frac{1}{2}(\widetilde{C} - \widetilde{I}) = \lambda_i^{2} - 1$ (EQ 3.9)

All members of the family produce identical strain values for infinitesimal deformations, but deviate from each other at large finite strain. Logarithmic strain is considered the most versatile measure of material strain as it does not have a definite upper limit to measurable strain, but is instead limited by mesh distortion.

The time rate of the deformation gradient ($\dot{\widetilde{F}}$) is utilised to determine the spatial velocity gradient ($\widetilde{L}$), the rate of strain ($\dot{\widetilde{\varepsilon}}$) and the spin ($\widetilde{\Omega}$) tensors. $\dot{\widetilde{F}}$ is multiplied by the inverse of the deformation gradient ($\widetilde{F}^{-1}$) in order to arrive at the spatial velocity gradient ($\widetilde{L}$). Hence:

$$\widetilde{L} = \dot{\widetilde{F}}\widetilde{F}^{-1} \qquad \text{(EQ 3.10)}$$

The velocity gradient consists of a rate of deformation and a rate of rotation or spin. Since these are rate quantities, we can treat the spin as a vector and hence decompose **(** $\tilde{L}$ **)** into a symmetric rate of strain matrix ($\dot{\tilde{\varepsilon}}$) and an anti-symmetric rate of rotation matrix ($\tilde{\Omega}$ **) (**Anon. 2002**)**. These quantities are given respectively as:

$$\dot{\tilde{\varepsilon}} = \tfrac{1}{2}(\tilde{L} + \tilde{L}^T) \qquad \text{(EQ 3.11)}$$

$$\tilde{\Omega} = \tfrac{1}{2}(\tilde{L} - \tilde{L}^T) \qquad \text{(EQ 3.12)}$$

The tensor fields described in this section each consist of four components, forming a simple 2x2 matrix in the chosen Cartesian coordinate system. The values of all four components for each tensor field are calculated for all nodes at all available times, and are stored in multi–dimensional arrays.

3.6.1.4 Material parameters

Initial material parameters are calculated according to the relevant constituent theory, based on the initial mass, volume and solids fraction of the experimental sample. As the sample is deformed, the value of the Jacobian (determinant of the deformation gradient) at each node changes accordingly. The Jacobian can thus be utilised as a multiplier of initial material parameters, to update the material parameters at each node. Hence, local material parameters such as void ratio, filling ratio, compaction, porosity and compression ratio are determined for each node in the analysis grid at all available times in the solution.

The ITA software prompts the user to input the initial mass and fibre content of the sample, along with the blanket feed height. Initial material parameters are determined and their transient counterparts evaluated at each time increment in the analysis and stored in multi-dimensional arrays.

3.6.2 Results post–processing

The ITA procedure has over 110 output variables, all of which are concurrent with finite element output. These include milling and porous media parameters, all components of the selected Doyle-Erickson strain tensors along with principal and volumetric strains for each measure, nodal velocities, principal stretch ratios and their

directions and the four components of the velocity gradient, rate of strain and spin tensors. Results are output in three files. The first file (stat.dat) outputs 12 chosen variables for graphical and statistical analysis in the form of a binary row-column data file. This file is easily imported into software packages such as Microsoft Excel© and S–Plus© for interpretation. The two remaining data files (grid.dat and results.dat) contain data for visualisation of results using the software package Fieldview©. The grid file contains the X, Y spatial locations of the nodes of the centre column of the analysis grid, at each increment in the solution; hence creating a spatial domain for display of the scalar and vector results from ITA. The method for construction of the visualisation grid is shown in Figure 3.6.

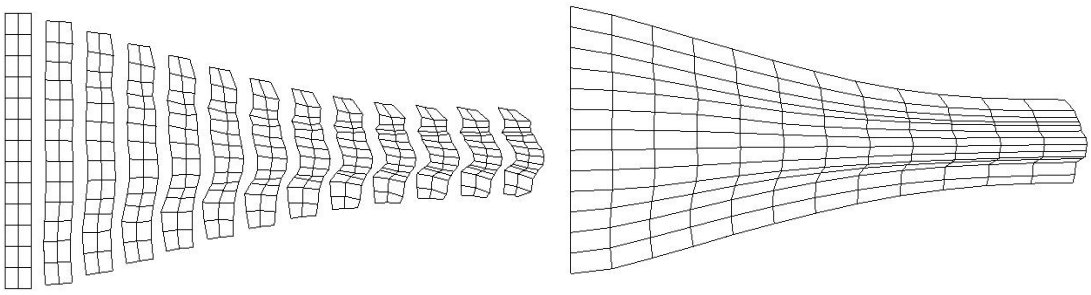

(a) (b)

Figure 3.6. Construction of the visualisation domain for two-roll milling results: a) The deformed analysis grid at selected time intervals in the analysis; b) Visualisation domain construction from the centre column of the deformed analysis grid at selected time intervals in the analysis.

The results file has 97 variable cells for storing results at each node in the visualisation grid. For example, one variable slot could contain the volumetric logarithmic strain at each node in the centre column of the analysis grid, for all increments in the solution. All the result slots are named according to the variable that they contain. Several FORTRAN routines were written in order to create a customised Fieldview data reader for the ITA grid and results files (Anon. 2000). These files provide the Fieldview software with the format of the data to be read, along with a list of the ITA results.

3.6.3 Extension of ITA software to transient uniaxial compression

Uniaxial compression experiments involving both flat and grooved platens have, for many years, allowed researchers to gain insight into bagasse compression, obtain material model parameters, and study the effects of varying groove geometry. The process of uniaxial compression is transient, involving the compression of a confined sample. Hence, the three–column grid adopted for ITA analysis of two-roll milling required modification, in order to accurately describe the deformation of a sample experiencing confined uniaxial compression. To obtain the full solution for the uniaxial compression regime, extension of the three-column grid to an n–row by m–column grid was implemented. The ITA software was appropriately modified to accommodate the larger analysis grid by introducing a parameter to depict the number of columns in the analysis grid. Furthermore, the software was modified to create grid and results files at each available time in the analysis, hence providing a basis to create animations of the measured transient deformation of experimental uniaxial samples. This method of output allows the user to construct the complete ITA kinematic solution of a given experiment and hence interpret the development of the strain field within the sample as time progresses. An example of visualised results from a uniaxial compression analysis is presented in Figure 3.7.

3.6.4 ITA interpolation software

Interpolation routines were implemented in the ITA software to smooth nodal abnormalities experienced by the grid during analysis. Instead of tracking the nodes in the moving (analysis) grid directly, a second, stationary grid was generated over the sample domain. The analysis grid was moved within this stationary grid, by interpolating each nodal displacement from the displacement values at the four surrounding points in the stationary grid. Simple linear weighting functions were applied to the displacement at the four surrounding stationary nodes, based on their proximity to the node of interest in the moving grid. This interpolation procedure is illustrated in Figure 3.8.

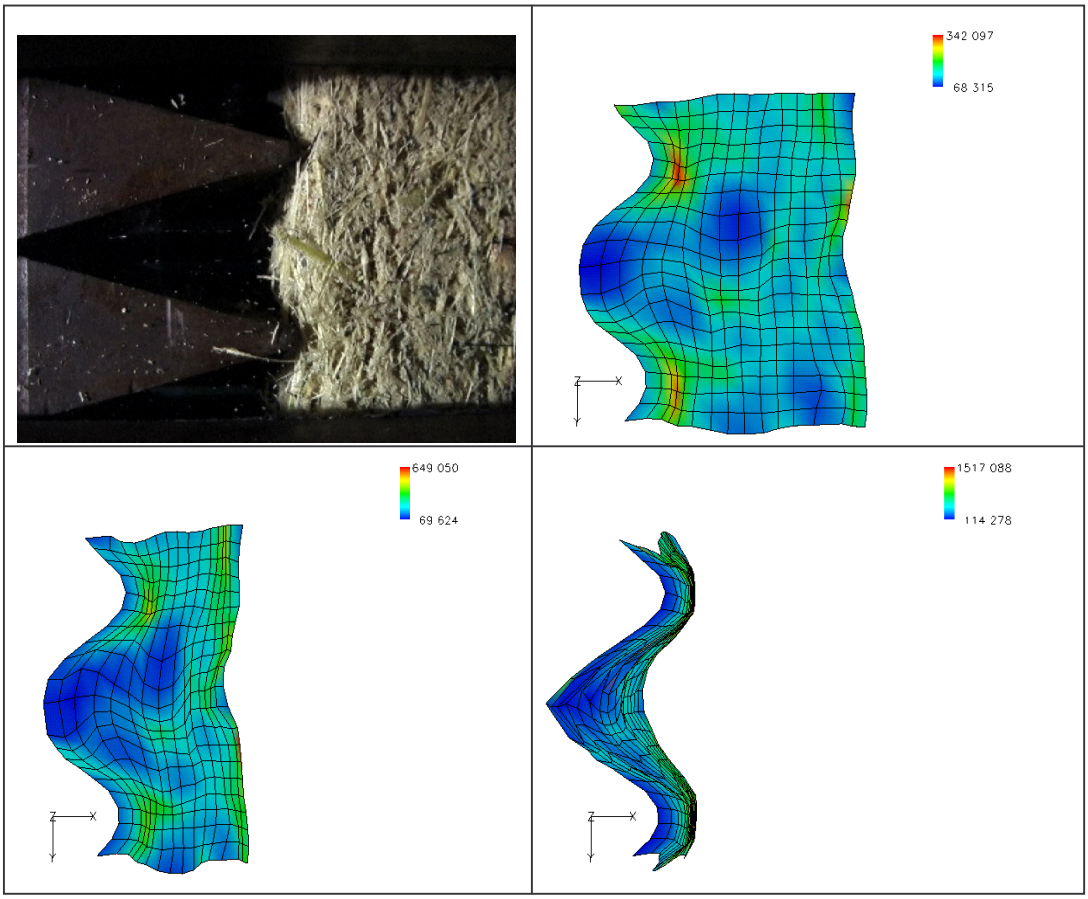

Figure 3.7. Visualisation of results at three selected times, taken from an ITA analysis of a uniaxial compression grooving experiment.

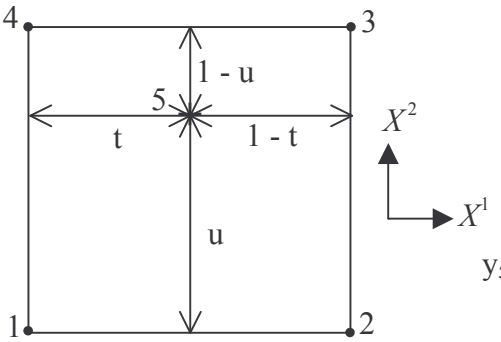

y - example interpolation variable

$$t = \frac{(x_5^1 - x_1^1)}{(x_2^1 - x_1^1)} \; ; \; u = \frac{(x_5^2 - x_1^2)}{(x_4^2 - x_1^2)}$$

$$y_5 = (1-t)(1-u)\, y_1 + t(1-u)\, y_2 + t\, u\, y_3 + u(1-t)\, y_4$$

Figure 3.8. Linear interpolation method: nodes 1 - 4 are in the stationary grid and node 5 is in the analysis grid.

3.6.5 Inherent assumptions of ITA

The ITA procedure was developed to provide kinematic and material outputs that are concurrent with finite element model output. The ITA procedure thus implies similar modelling assumptions to the FEM procedure. Firstly, motions are assumed smooth

and thus continuously differentiable, inferring that the fibre blanket maintains a material continuum during the motion. The initial fibre density is assumed to be uniform across the depth of the material samples, as no means for measuring local fibre density is currently available. Finally, the ITA procedure is only applicable in plane strain scenarios, where the deformation of the sample surface closely represents the deformation of the entire sample (flat–roll milling, uniaxial compression and direct shear experiments).

3.6.6 Improving ITA measurements at external boundaries

External boundaries such as platen and roll surfaces were identified to significantly influence displacement measurements for material in these regions. As a node approaches an external boundary, the sub–region centred on the node will overlap this surface. When the overlap exceeds approximately one–quarter of the subregion size, the surface basically prevents the node from further displacement. The image measurement resolution in these regions is thus dependent upon the size of the nodal sub–regions.

3.6.6.1 Sample seeding

In PIV analyses of fluid flow, neutrally buoyant seed particles are placed in the fluid for flow visualisation. Laser illumination is often used to show the particles as white against a black fluid background, or vice versa. This provides ideal contrast for the FFT algorithm to measure the average particle displacements within sub–regions. Unlike transparent fluids, bagasse is an organic fibrous material, whose grey–scale appearance under suitable lighting, varies significantly. Black dyed bagasse fibre provides a means of seeding samples without altering the material properties. This material seed enhances the contrast in the grey–scale image, and improves the FFT measurement success, over the entire sample surface.

3.6.6.2 Numerical image masking

Numerical masking (or padding) of external boundaries is often conducted to set the pixel values of these boundaries to the background colour in the images. Such techniques are widely used (Raffel et al. 1998, Stephens 1996) in fluid analyses, where the fluid provides uniform background pixel values. The pixels on the external boundaries are thus numerically assigned the background value, making the

boundaries disappear. The masking routines developed as part of this study, are described in Appendix B, and allow masking of both circular roll, and flat or grooved platen surfaces, with minimal user input. The routines allow numerical image masking of pixels with any grey–scale pixel value. The most common pixel value of regions occupied by material is determined for a given image series using the NIH Image© software, and used to mask the boundary regions according to the user inputs. The image masking provided an improvement in the ability to track nodes closer to the external roll and platen boundaries. However, comparison with manual measurements of image displacements, conducted using the NIH Image© software, still showed discrepancies in the improved ITA measurements. Hence, a numerical technique based on size reduction of sub–region was created within the ITA routine, as an alternative means to solve this boundary problem.

3.6.6.3 Sub–region reduction

A sub–region reduction routine was created in the ITA software that allowed the size of the sub–region to decrease, as nodes approached an external boundary. At any time increment in an ITA analysis, if the sub–region associated with a node comes within one pixel of an external boundary, its dimensions are reduced to the next integer power of two. For example, if a node with an associated sub–region of 64 pixels by 64 pixels comes within 33 pixels ($64/2 + 1$) of an external boundary, the sub–region size is reduced to 32 pixels by 32 pixels. The sub–region will then remain this size, until it again comes within one pixel of the boundary, and is further reduced to 16 pixels by 16 pixels. This technique is suitable for situations where the incremental displacement is sufficiently low, that reduction of the sub–region size does not result in reduced particle tracking accuracy.

3.6.7 Software calibration

In order to obtain accurate displacement and derivative measurements with the ITA procedure, suitable values of particle tracking parameters and node spacings must be determined for the materials of interest. Using the NIH Image© software to manually measure the displacements of nodal locations within the samples, provides a suitable method of assessing the accuracy of the particle tracking algorithm for various combinations of parameters. Node spacing calibration is to be conducted by assessment of deformation predictions, over a wide range of node spacing values.

Confined uniaxial flat–platen compression experiments provide a simple loading scenario for calibrating the ITA procedure, to obtain accurate deformation mappings of prepared cane and bagasse samples.